Hierarchically Structured Co@$Fe_{(SA)}$-MoO/MoP Electrocatalyst with Tuned Electronic States for Thermodynamically Optimized Hydrogen Adsorption in Chloride-Rich Media

Muhaiminul Islam[a], Jong woo Hong[a], Kanguk Park[b], Amar M. Patil[a], Taehyeon Kim[a], Sushanta K. Das[a], Seungho Yu[b], Seong Chan Jun [a, *].

[a]Nano-Electro-Mechanical Device Laboratory School of Mechanical Engineering, Yonsei University, Seoul 120-749, South Korea

[b]Energy Storage Research Center, Korea Institute of Science and Technology, 5, Hwarang-ro 14-gil, Seongbuk-gu, Seoul 02792, Republic of Korea

*Corresponding Author

Prof. Seong Chan Jun

Email- scj@yonsei.ac.kr

Material characterization and electrochemical analysis

The morphological and structural characteristics of the developed catalysts were investigated using scanning electron microscopy (SEM) with the model MIRA3 TESCAN at Yonsei University (South Korea) and transmission electron microscopy (TEM) on a JEM-F200 (Japan) at the Yonsei University Joint Research Center (South Korea). Surface chemistry analysis was conducted using X-ray photoelectron spectroscopy (XPS) with a K-Alpha instrument (Thermo Fisher Scientific, UK) at the Structural Analysis Division of the Yonsei University Joint Research

Center. The survey spectrum was calibrated by referencing the C1s peak, which was fixed at 284.8 eV. Peak deconvolution of the XPS spectra was performed using the Peak Fit software. The peak positions were assigned based on standard photoelectron emission data from the National Institute of Standards and Technology (NIST) X-ray Photoelectron Spectroscopy Database (Standard Reference Database 20, Version 5.0). The crystalline properties of the catalysts were examined via X-ray diffraction (XRD) analysis, of Rigaku diffractometer (Maxima XRD-7000) utilizing a Cu–Kα radiation source (λ = 0.15406 A.U.), also at the Yonsei University Joint Research Center.

Electrochemical performance evaluations were performed in a three-electrode cell connected to an IVIUMnSTAT multichannel electrochemical workstation. The synthesized materials (1 cm × 1 cm), a graphite rod (Diameter 3.05mm with 99.9995% metal basis, ultra "F" purity), and a saturated Ag/AgCl (3.0 M KCl) electrode were used as the working, counter, and reference electrodes, respectively. To study OER/HER activities, Linear sweep voltammetry (LSV) measurement was performed at a scan rate of 2.0 mV s^{-1} in alkaline freshwater medium (1.0 M KOH, pH~14), natural seawater and simulated seawater (1.0 M KOH +0.5 M NaCl, pH~12.9). Natural seawater(pH~13.2), filtered multiple times, was supplemented with 1.0 M KOH and stirred for 24 h. All electrolytes were saturated by the N_2 gas for 15 min before the experiments. The obtained linear sweep voltametric was corrected by the iR (~90%) compensation for the HER and OER following the equation[1]

$$E_{iR-corrected} = E_{(vs.RHE)} - i \times Rs \ldots\ldots\ldots\ldots\ldots\ldots (i)$$

(Where, 'i' and 'Rs' are the current and resistance of the electrolytic solution respectively).

The as obtained potential was switch to RHE (Reversible hydrogen electrode) potential using formula [2];

$$E_{RHE} = E_{Ag/AgCl} + 0.098 + 0.059pH \ldots\ldots\ldots\ldots (ii)$$

Stability of electrodes was examined by chronoamperometry at a fixed overpotential (η) to achieve an initial current response of ~50 mA cm^{-2} and ~100 mA cm^{-2}. The cyclic voltammetry (CV) was conducted at various scan rates from 10 to 100 mV s^{-1} to estimate the double-layer capacitance (C_{dl}) that is associated with the electrochemical surface area (ECSA) of the synthesized catalysts by following equations [3,4].

$$C_{dl} = Ja - jc/2 \ldots\ldots\ldots\ldots\ldots\ldots (iii)$$

Where, j_a and j_c is the anodic and cathodic voltametric current density.

$$ECSA = C_{dl}/C_s \ldots\ldots\ldots\ldots\ldots\ldots (iv)$$

Where C_{dl} and C_s are double-layer capacitance and specific capacitance of a flat surface respectively.

The Faradaic efficiency for water splitting catalyzed by $Co@Fe_{(SA)}$-MoO/MoP was computed by dividing the experimentally generated gas quantity by the theoretically calculated gas amount, determined through the charge passed through the electrode[5] :

Faradaic efficiency (ηF)

$$\eta F = \frac{n.F.V\ measurement}{(I \cdot t \cdot Vm)} \ldots\ldots\ldots\ldots\ldots (v)$$

where ηF is the faradaic efficiency, n is the number of exchanged electrons in the reaction, F is the Faraday constant, V measurement is the volume of the measured H_2 or O_2 gas, I is the applied current, t is the electrolysis time, and Vm is the molar volume (22.4 dm^3 mol^{-1}). Electrochemical

impedance spectroscopy (EIS) technique was studied by applying 5 mV amplitude AC voltage in the frequency range (0.01 Hz to 100 kHz), to evaluate the charge transfer resistance of the electrodes. For comparison of electrochemical performance, commercial Pt/C and RuO_2 catalysts on carbon cloth (CC)-based electrodes were prepared. In this process, Pt/C (20 wt.% Pt) or RuO_2 (15 mg), equivalent to the loading of Co@$Fe_{(SA)}$-MoO/MoP on CC (1 cm × 1 cm), was dissolved in 500 µL of pure ethanol containing 10 µL of Nafion (5 wt.%) under continuous sonication for 40 minutes. The resulting ink was applied to both sides at dropped wise by the drop casting method of the CC substrate (1 cm × 1 cm) and dried under vacuum at 60 °C overnight before being used for electrochemical characterization.

Turnover frequency (TOF) evaluation.

To calculate the TOF, cyclic voltammetry (CV) curves for various fabricated materials were recorded at a scan rate of 10 mV s^{-1} in a 1.0 M PBS solution with a pH of approximately 6.5 (Figure S15).The absolute values of the cathodic and anodic voltametric charges recorded during a single measurement were summed. The quantity of active species (n) was then determined using the following equation [6]:

$$n = \frac{Q}{2F} = \frac{It}{2F} = \frac{IV}{2Fv} \quad \text{.....(vi)}$$

Then, TOF (s^{-1}) is calculated following equation:

$$TOF = \frac{|j|A}{nmF} \quad \text{.....(vii)}$$

Here, Q represents the voltammetric charge, F is the Faraday constant (C mol^{-1}), III is the current density (A cm^{-2}), ttt is time (s), V is the voltage (V), v is the scan rate (V s^{-1}), jjj is the current (A)

recorded during linear sweep voltammetry (LSV) tests, A is the electrode area (1 cm^2), and mmm denotes the number of electrons required to produce one molecule of H_2 or O_2 from H_2O. For the HER and OER, m is vi and vii, respectively.

Assembly of Anion exchange membrane water electrolysis(AEMWE) assembly

AEMWE devices were assembled using a 4.5 × 4.5 cm^2 configuration. Co@Fe(SA)-MoO/MoP was used as both the anode and cathode catalyst. For comparison, commercial RuO_2 and Pt/C (5 wt%) were dispersed in isopropanol with 5 wt% Sustainion XA9 ionomer and ultrasonicated for 1 hour to prepare catalyst inks, which were then air-brushed onto gas diffusion layers to achieve the desired loadings. A PiperION® 40 μm self-supporting anion exchange membrane and gas diffusion layers (carbon cloth and stainless-steel fiber felt) were employed in the assembly. A 1.0 M KOH electrolyte was circulated through both electrodes at 2 mL min^{-1}. Polarization curves were recorded potentiodynamically at 5 mV s^{-1}, and durability tests were conducted under continuous water electrolysis. All data are presented without iR correction.

Computational methods

First-principles calculations were conducted using the projector-augmented wave method[7] and the Perdew-Burke-Ernzerhof (PBE) generalized gradient approximation [8], as implemented in the Vienna Ab Initio Simulation Package (VASP)[9]. The calculations were carried out using a plane wave basis set with a cutoff energy of 520 eV, along with a gamma-centered 2×2×1 grid for k-point sampling. The electronic self-consistency and ionic relaxation loops were converged to thresholds of 10-5 eV and 0.03 eV/Å, respectively. All calculations were spin-polarized, and Van der Waals (vdW) interactions were incorporated using the DFT-D3 correction method[10]. The

calculations were conducted using the experimentally observed MoO2(-111) and MoP(101) slabs. The hydrogen adsorption energy was determined using the equation E_(ads_H)=E_All-E_Substrate-1/2E_(H_2), where E_All, E_substrate, and E_(H_2) represent the total energies of the complete system, the substrate, and the H_2 molecule, respectively. The Gibbs free energy for the hydrogen evolution reaction (HER) was evaluated using the equation ΔGH* = ΔEads + ΔEZPE – TΔS, where ΔEads represents the hydrogen adsorption energy on the slabs (H*), and ΔEZPE and ΔS correspond to the zero-point energy and entropy differences between the free and adsorbed states, respectively. The density of states (DOS) was obtained to investigate the electronic properties.

Battery Performance Test

The cell measurements were performed using a standard two-electrode system, with the prepared catalysts serving as the cathode and a Zn foil plate as the anode in a 1.0 M KOH electrolyte. Polarization curves were recorded at a scan rate of 5 mVs^{-1} using a ZIVE potentiostat, and power density curves were derived from the polarization data. Long-term stability was assessed through chronoamperometry discharge testing at 10 mA cm^{-2} in both alkaline seawater and 1.0 M KOH electrolyte.

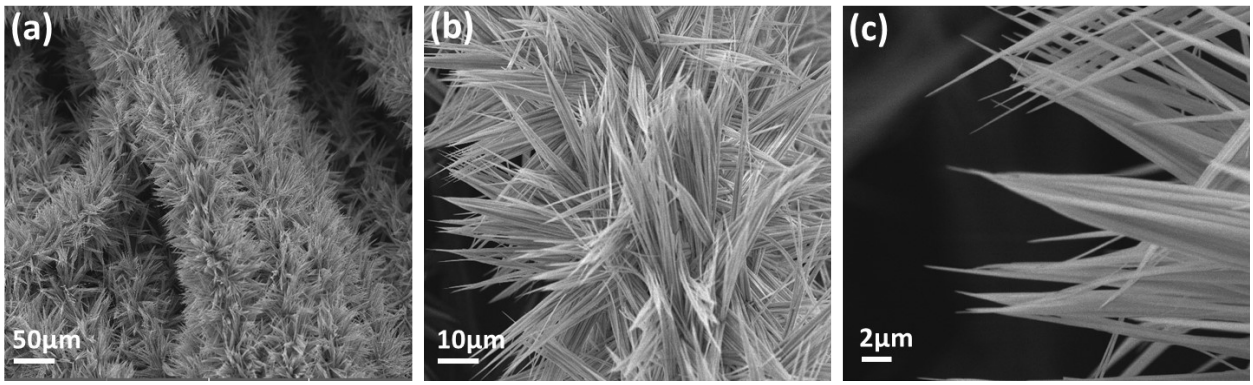

Figure S1.(a-c) SEM images of Co-OH NRs grown on CC substrate.

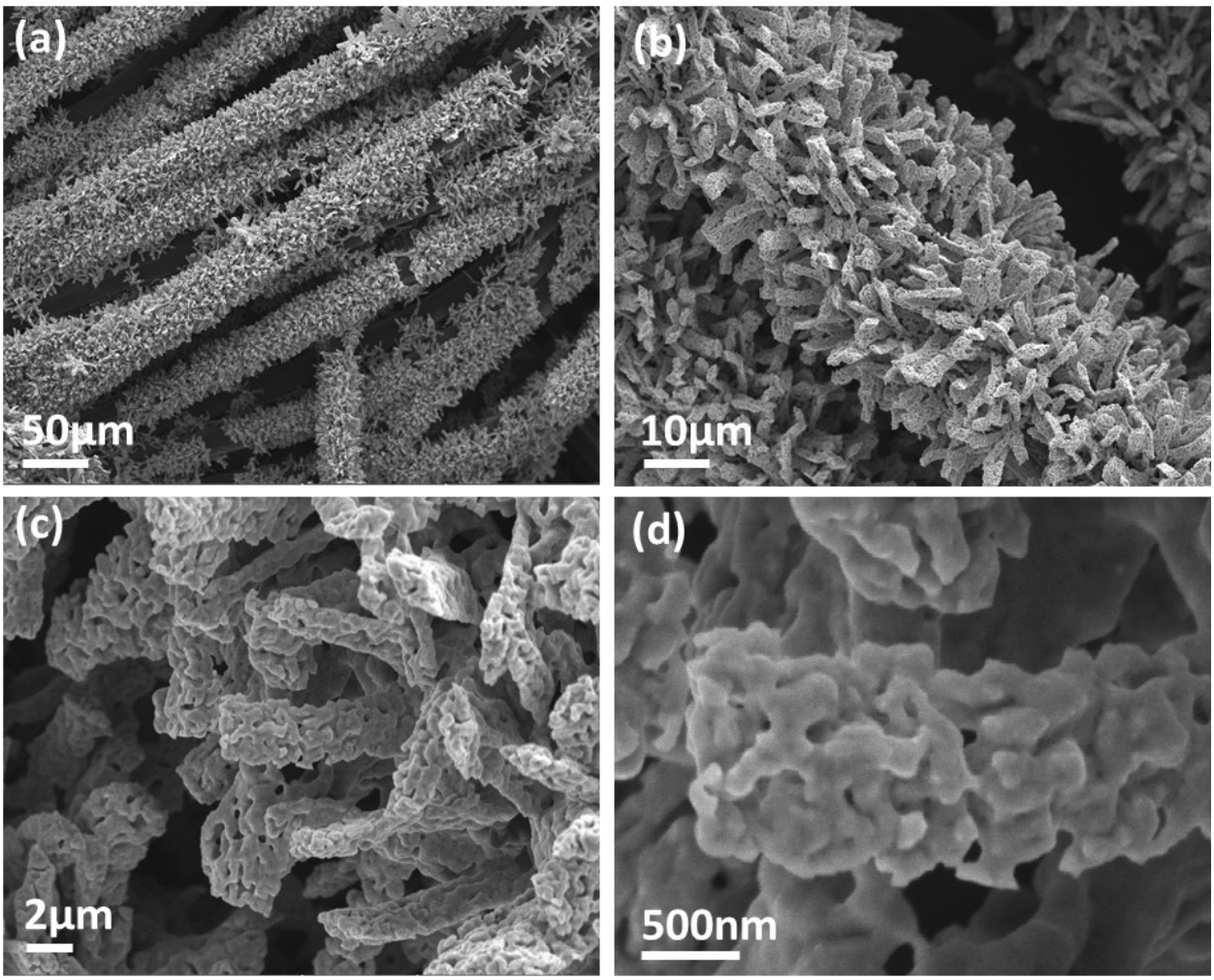

Figure S2.(a-d) SEM images of Co NRs grown on CC substrate after thermal treatment.

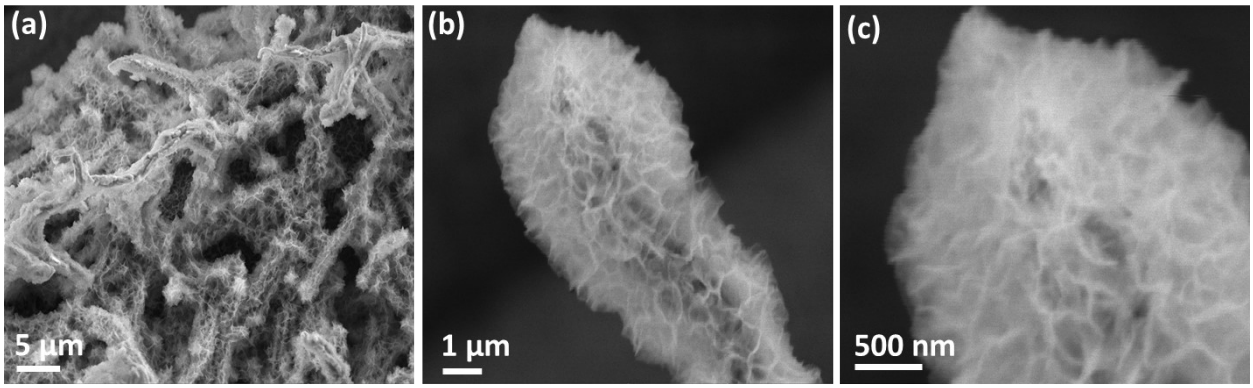

Figure S3.(a-c) SEM images of Co@MoO_x grown on CC substrate.

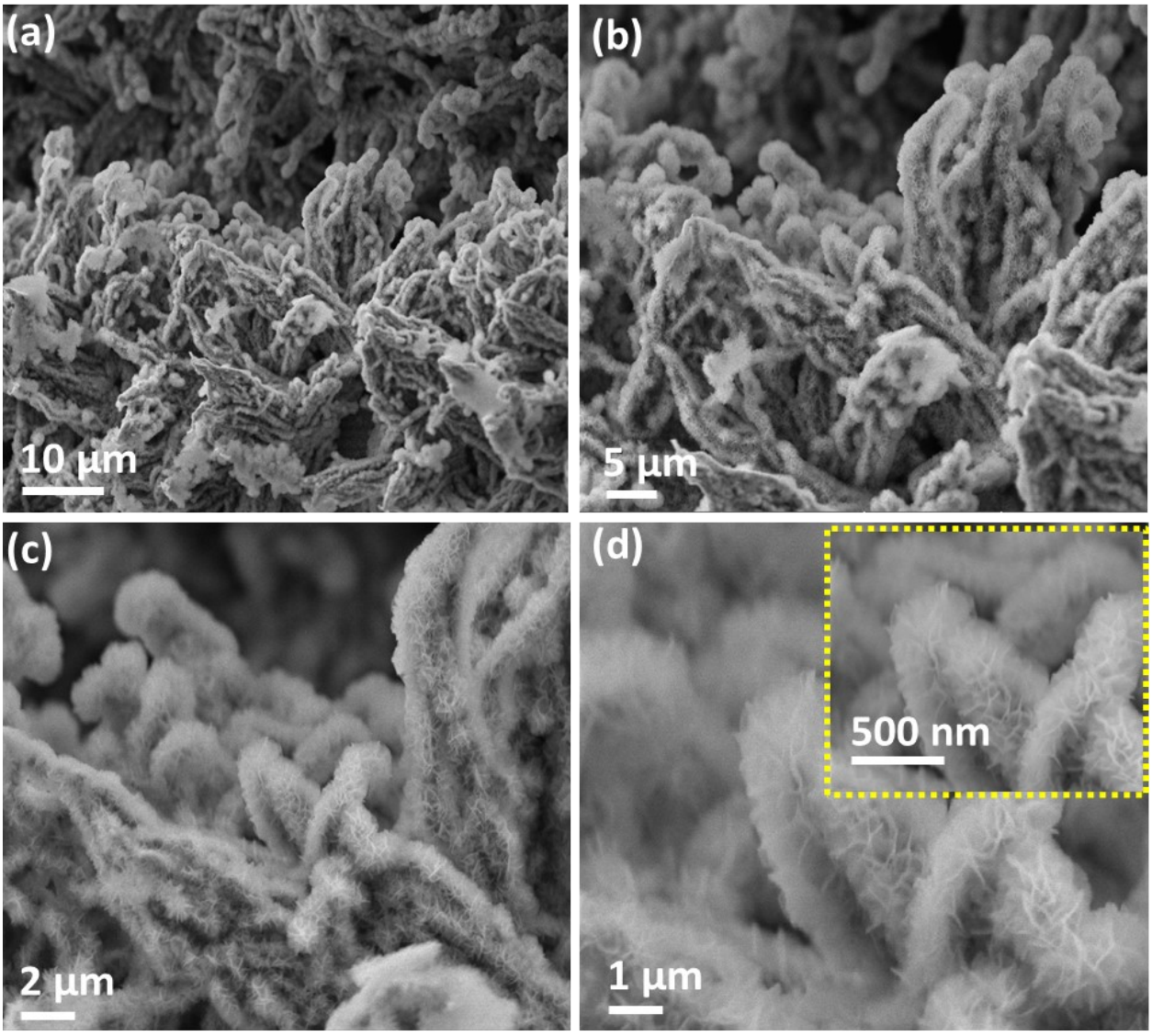

Figure S4.(a-d) SEM images of Co@$Fe_{(SA)}$-MoO/MoP grown on CC substrate.

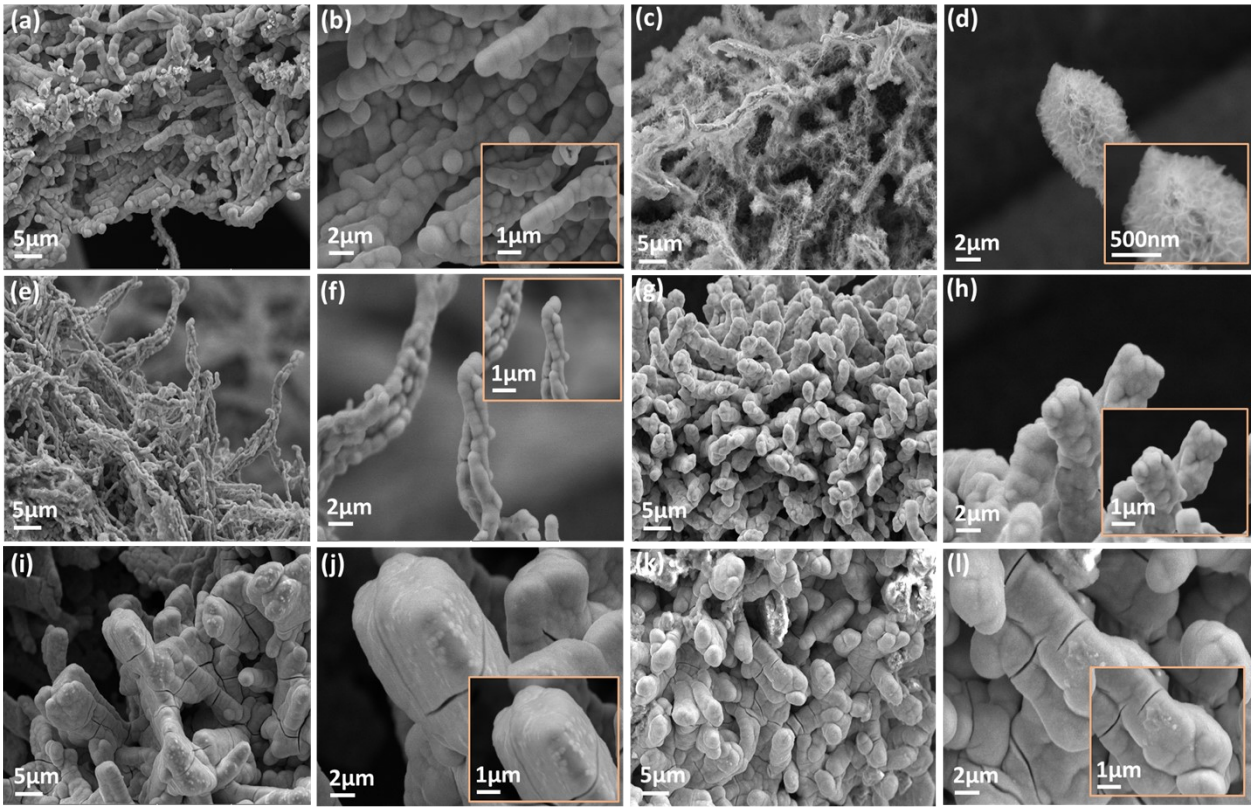

Figure S5.(a-b) SEM images of different time grown of MoO_x on Co NRs on CC substrate.

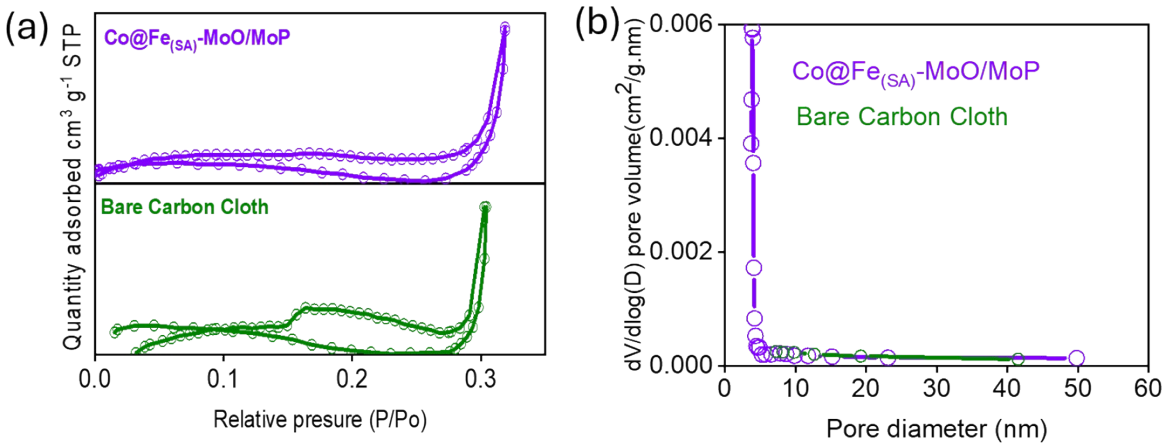

Figure S6. Nitrogen adsorption-desorption isotherms of (a) Co@$Fe_{(SA)}$-MoO/MoP and bare carbon cloth; (b) Pore size distribution of Co@$Fe_{(SA)}$-MoO/MoP and bare carbon cloth

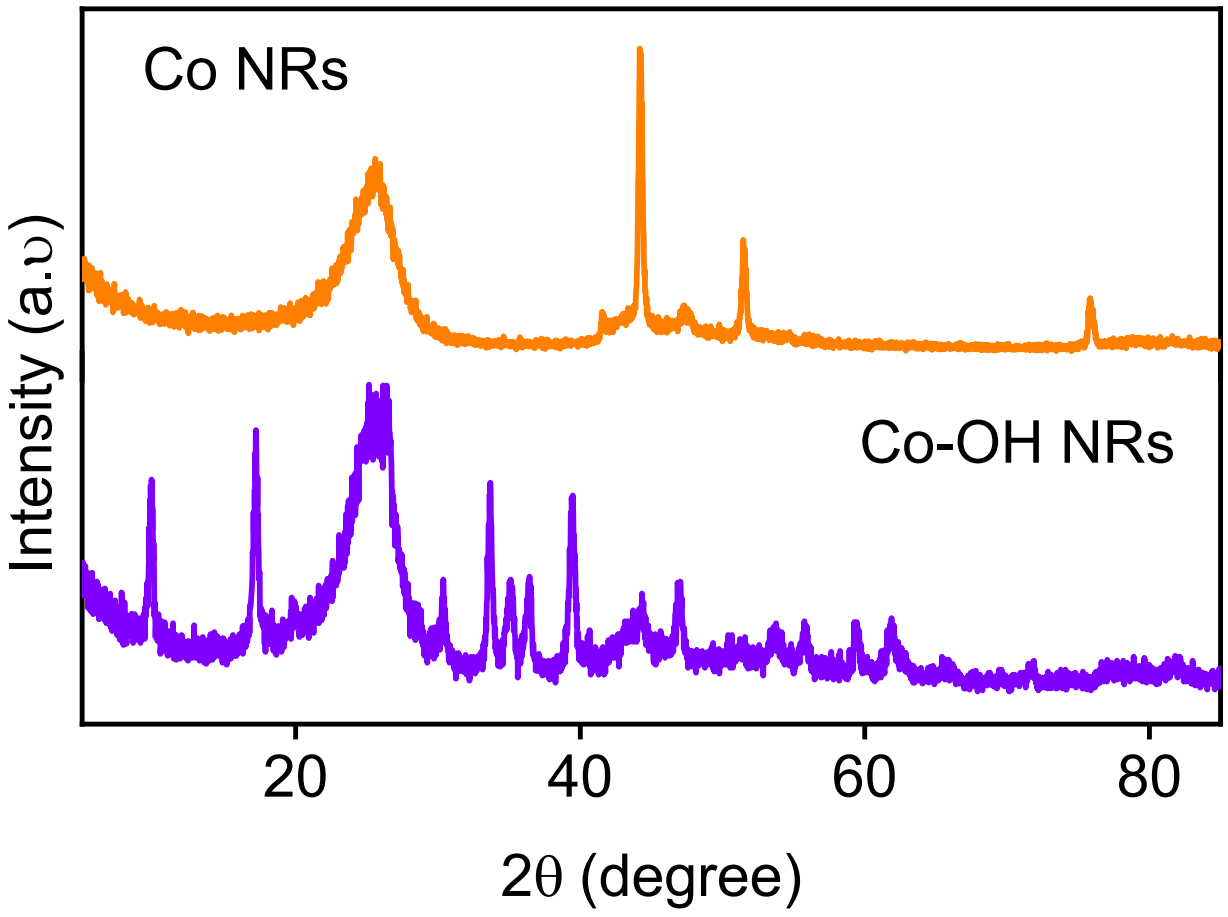

Figure S7.XRD analysis of Co NRs and $Co(OH)_2$ NRs prepared on CC.

209

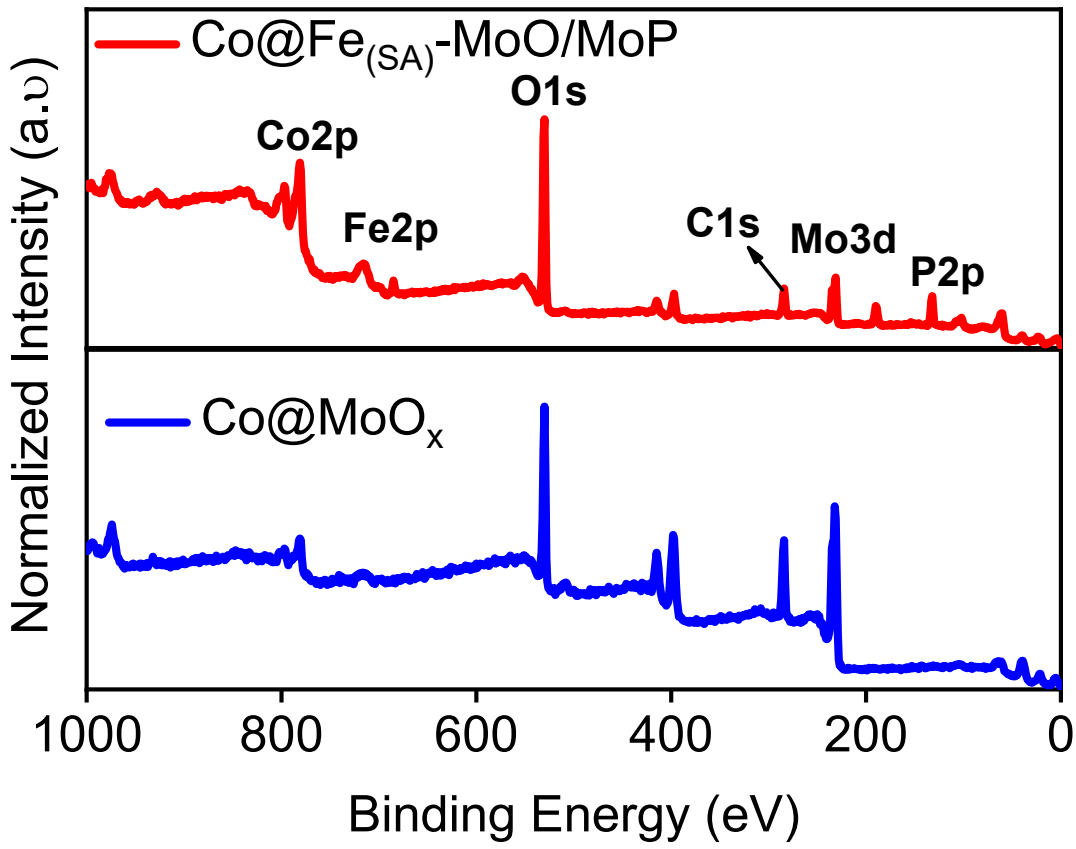

210

211 **Figure S8.**XPS survey scans of Co@$Fe_{(SA)}$-MoO/MoP and Co@MoO_x prepared on CC.

212

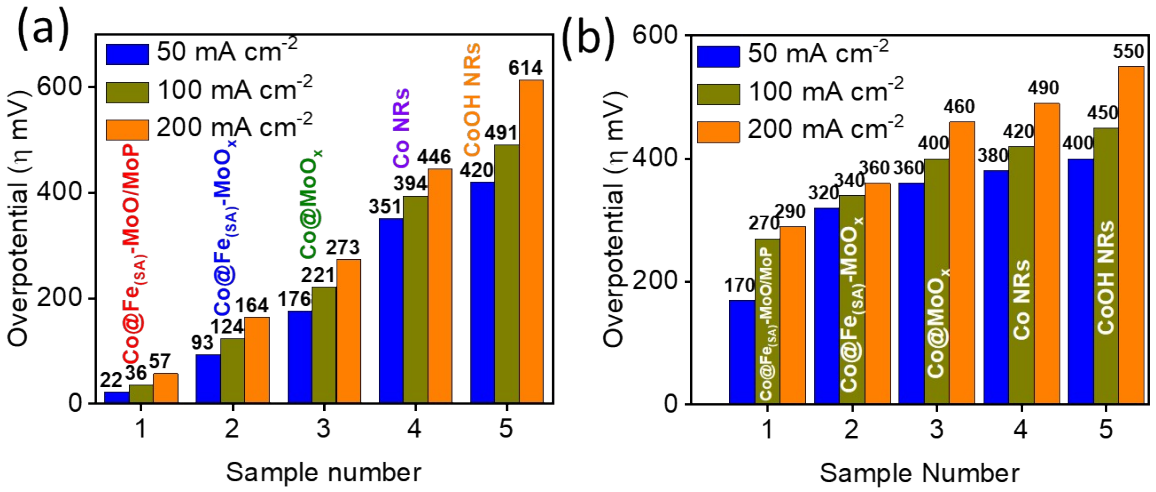

Figure S9. Overpotential comparison of the prepared samples towards (a) HER and (b) OER measured at 50, 100 and 200 mA cm^{-2} current density in an alkaline freshwater environment.

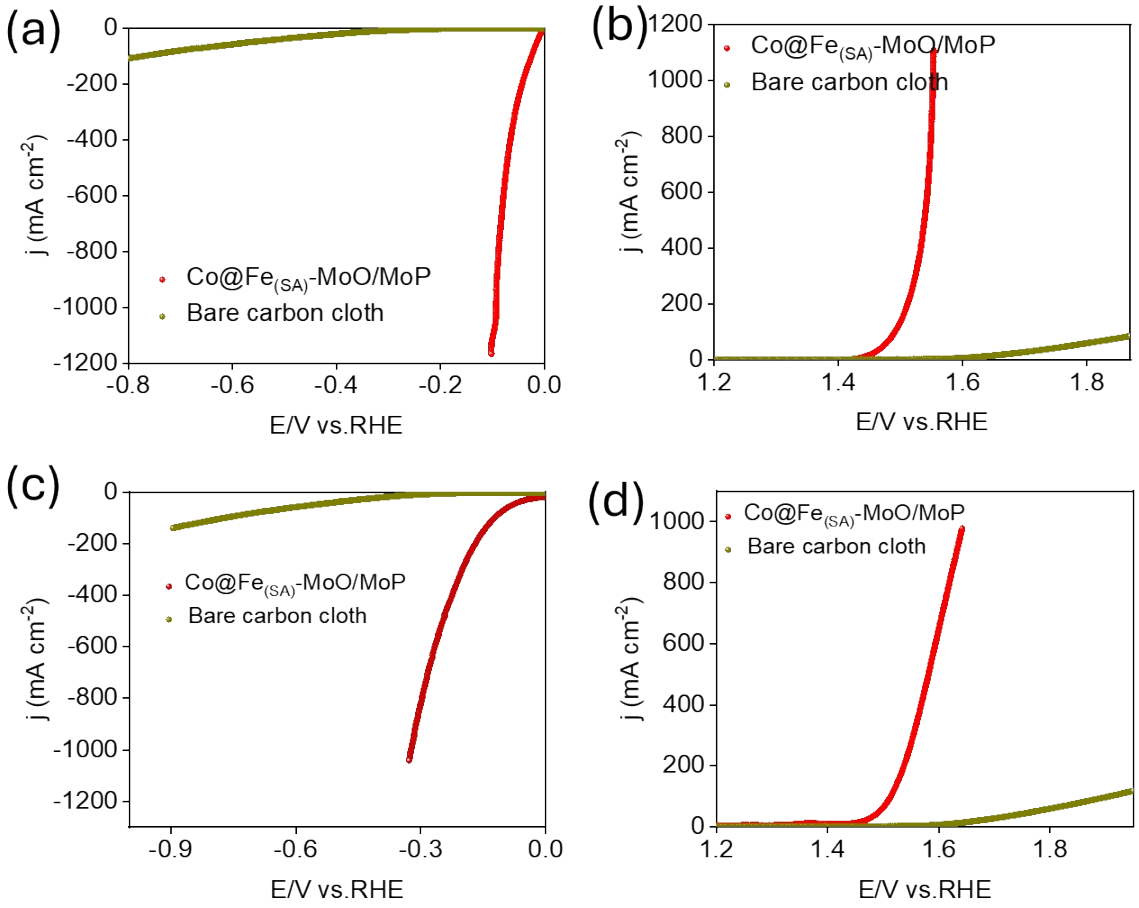

227

228

229 **Figure 10.** Comparison of (a-c) HER and (b-d) OER performance between Co@$Fe_{(SA)}$-MoO/MoP
230 and bare carbon cloth in (a-b) 1.0 M KOH and (c-d) natural seawater electrolytes.

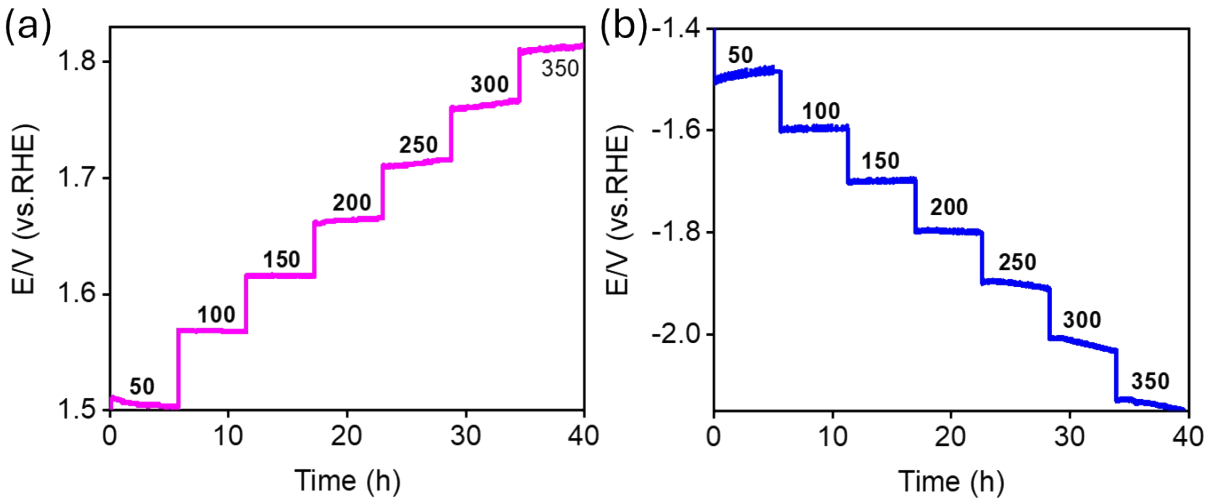

Figure S11. Multi-step stability of the Co@$Fe_{(SA)}$-MoO/MoP (a) HER and (b) OER in an alkaline environment (1.0 M KOH).

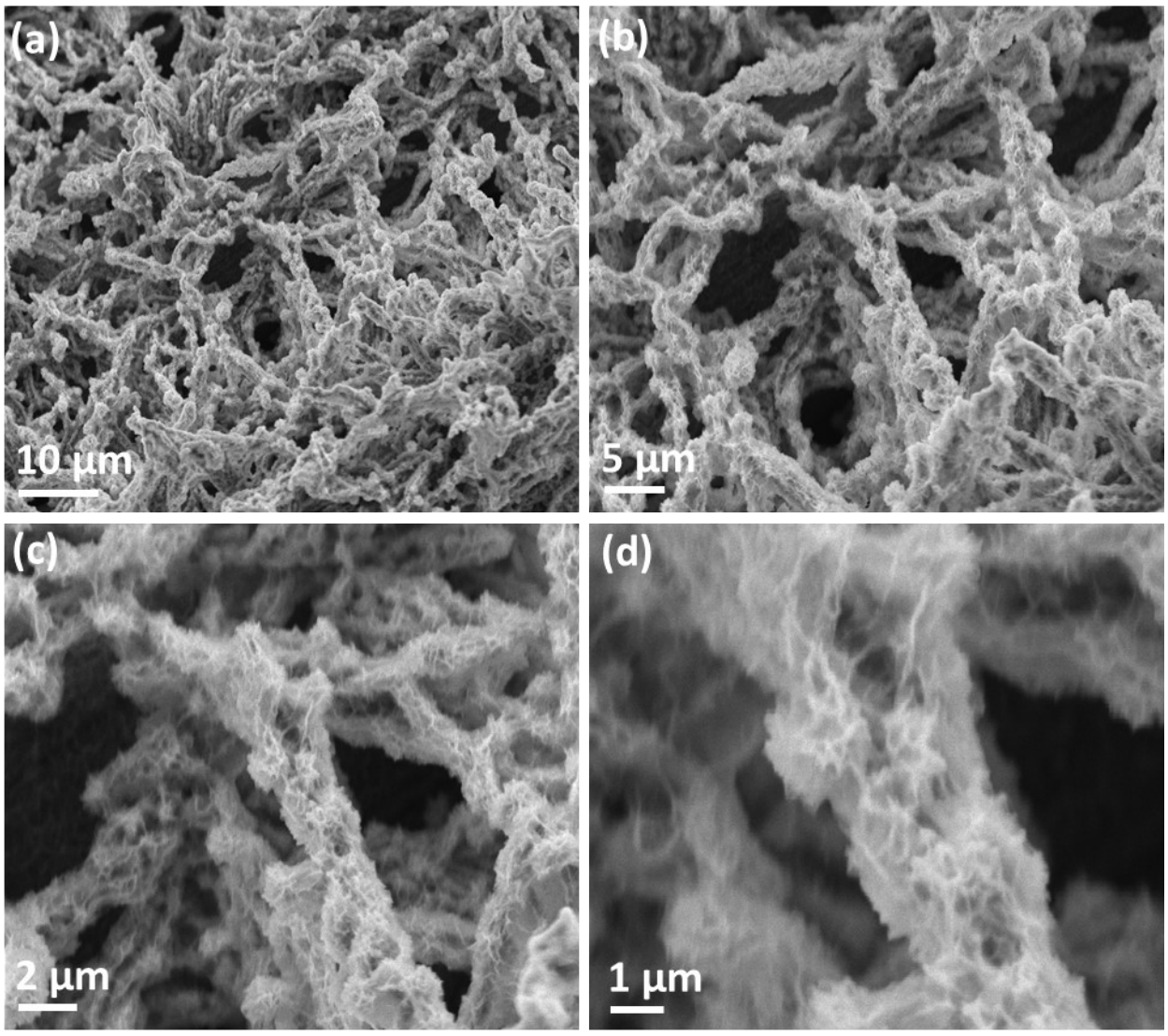

Figure S12. (a-d) FE-SEM images of the Co@$Fe_{(SA)}$-MoO/MoP after HER stability tests at 100 mA cm^{-2} current density

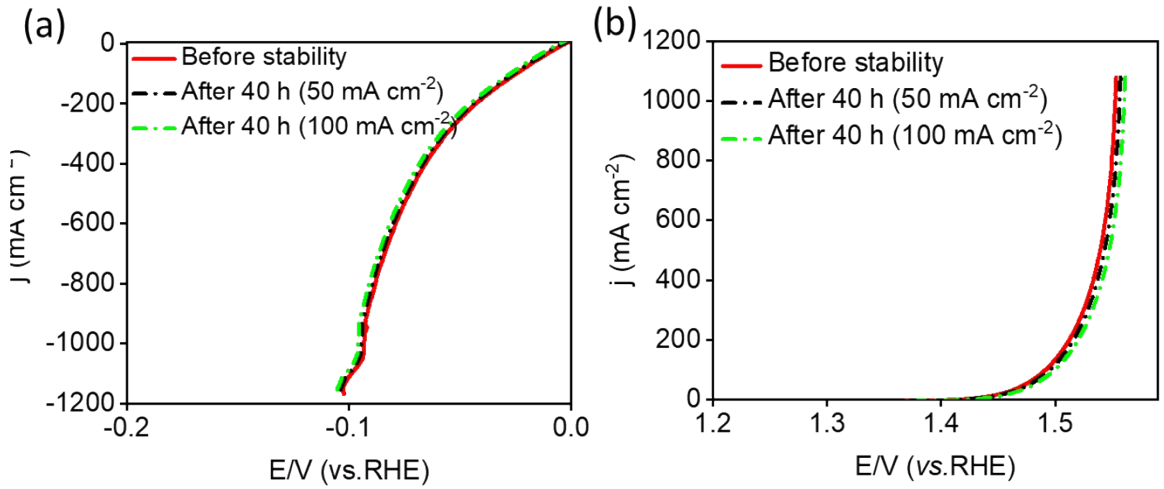

Figure S13.(a) HER and (b) OER LSV curves of the Co@$Fe_{(SA)}$-MoO/MoP measured after long-term stability tests conducted at 50 mA cm^{-2} and 100 mA cm^{-2} current density, respectively

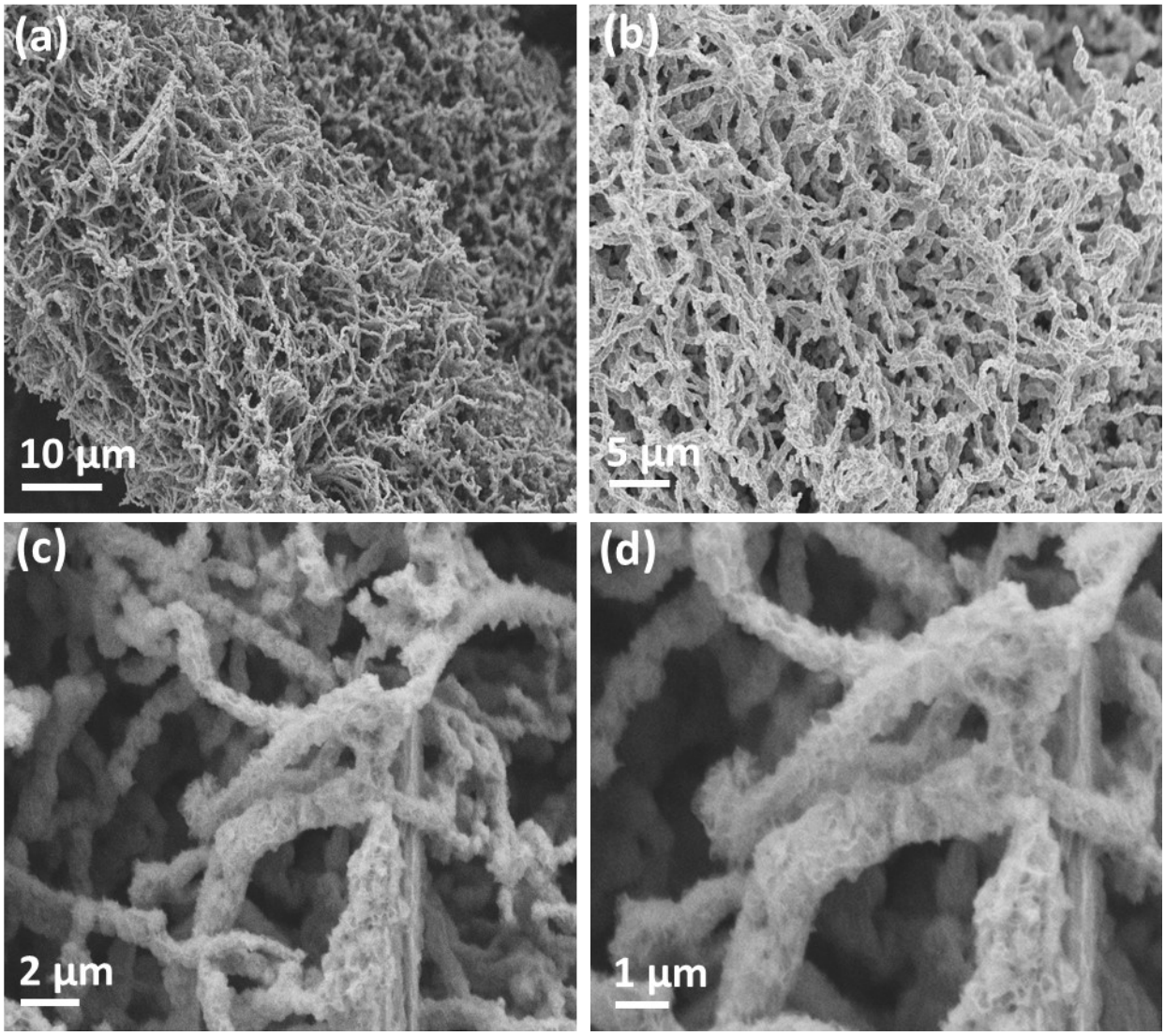

Figure S14.(a-d) FE-SEM images of the Co@$Fe_{(SA)}$-MoO/MoP after OER stability tests at 300 mA cm^{-2} current density

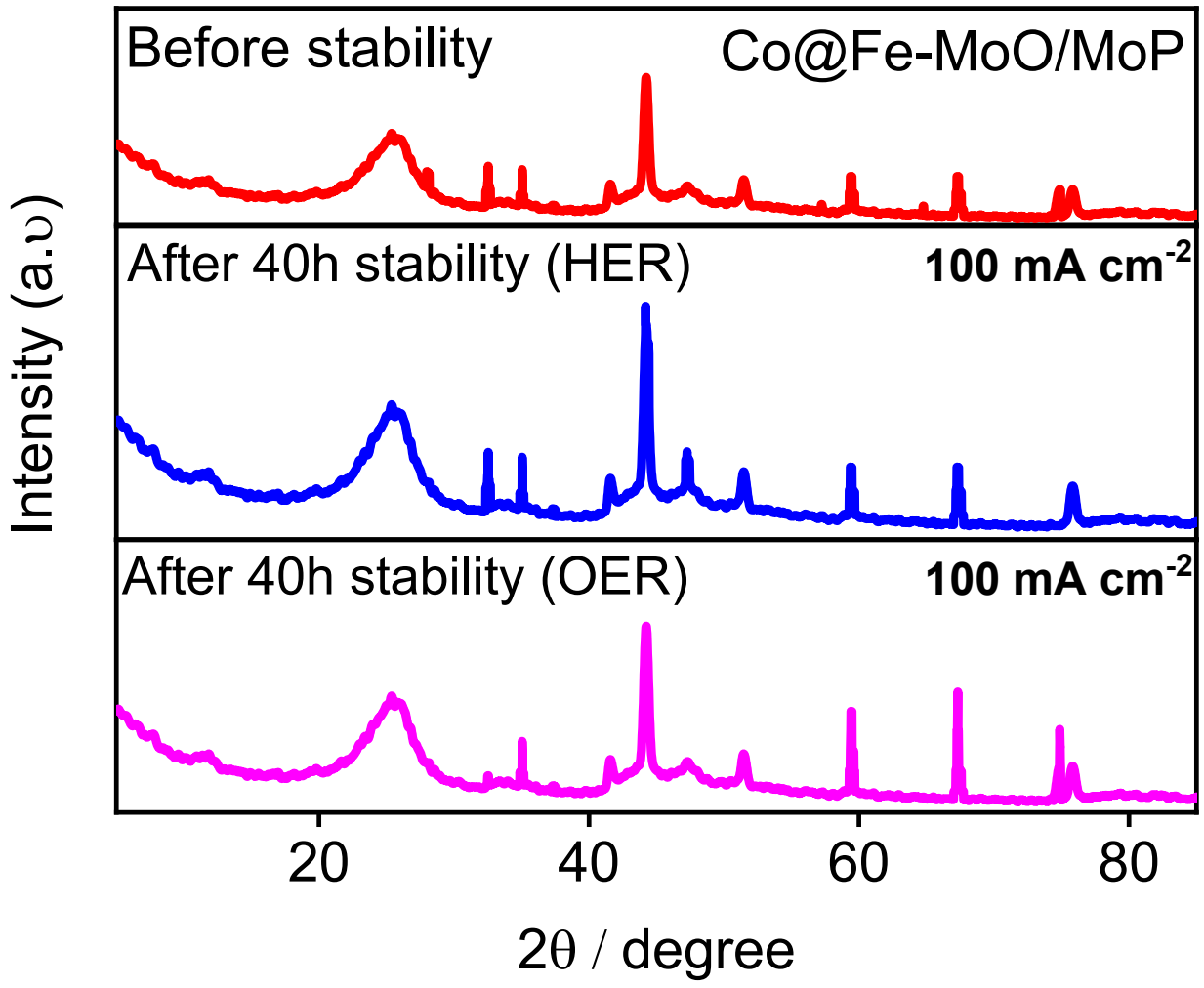

Figure S15. (a)) XRD patterns of Co@$Fe_{(SA)}$-MoO/MoP sample before and after long-term HER/OER stability tests conducted at 100 mA cm^{-2} current density;

293

294

295

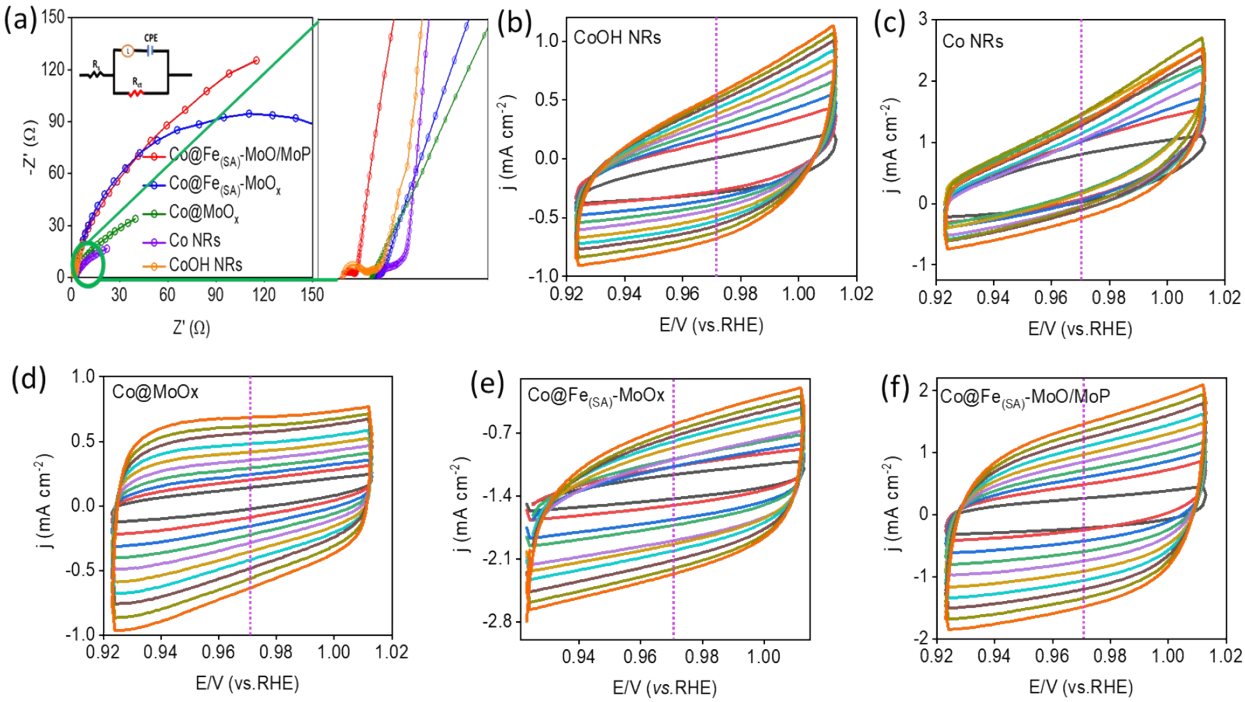

296

297 **Figure S16.** (a)Nyquist Plots from EIS Measurements in 1.0 M Alkaline Electrolyte with Enhanced

298 Resolution, .(b-f) CV curves of prepared samples measured between 10 to 100 mV s-1 scan rate

299 in alkaline electrolyte (1.0 M KOH).

300

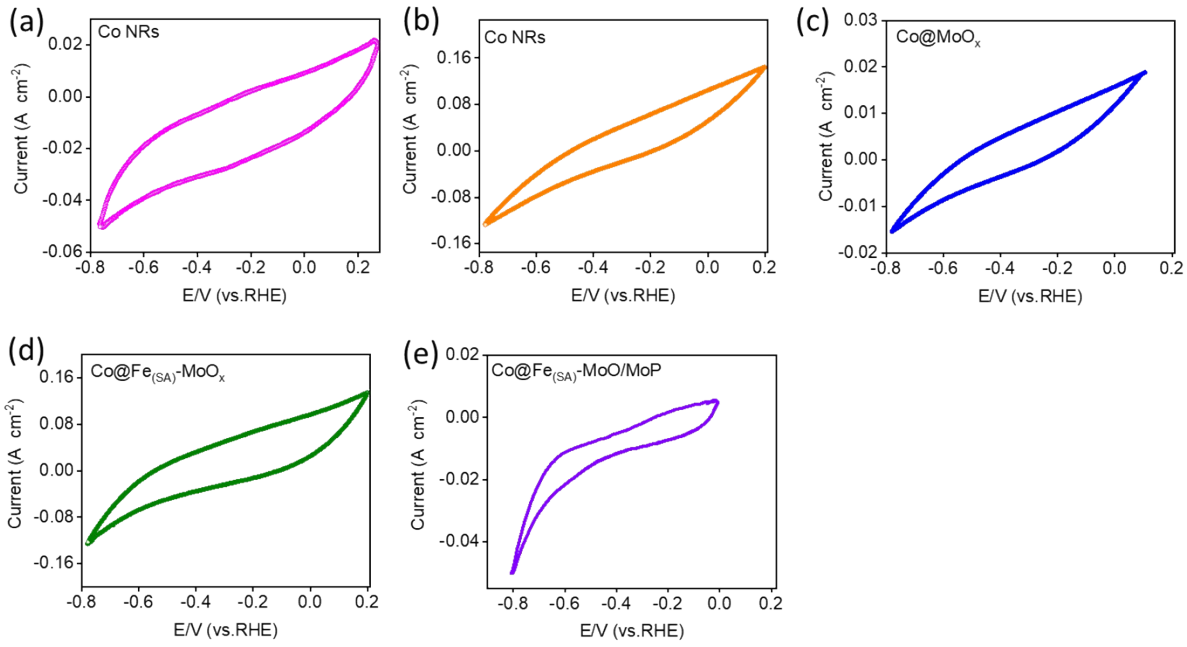

Figure S17.(a-e) CV curves of prepared samples measured at scan rate 10 mV s^{-1} scan rate in 1.0 M PBS electrolyte.

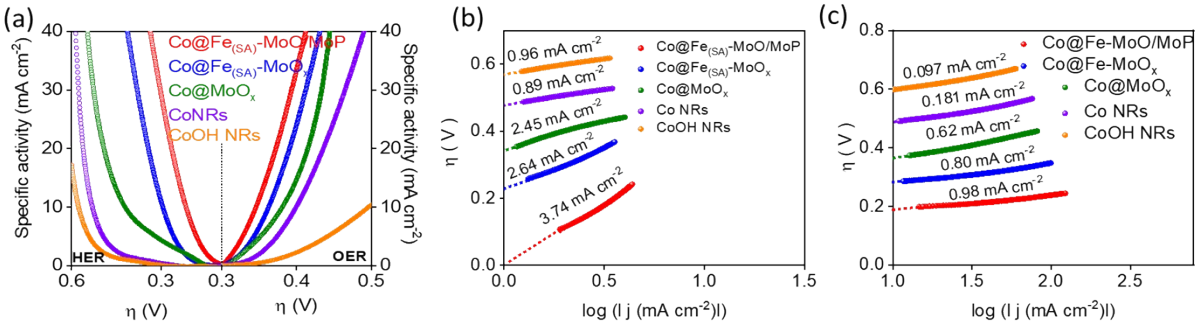

Figure S18. (a) TOF, analysis of the developed catalysts. (b)The exchange current density of Co@$Fe_{(SA)}$-MoO/MoP in 1.0 M KOH

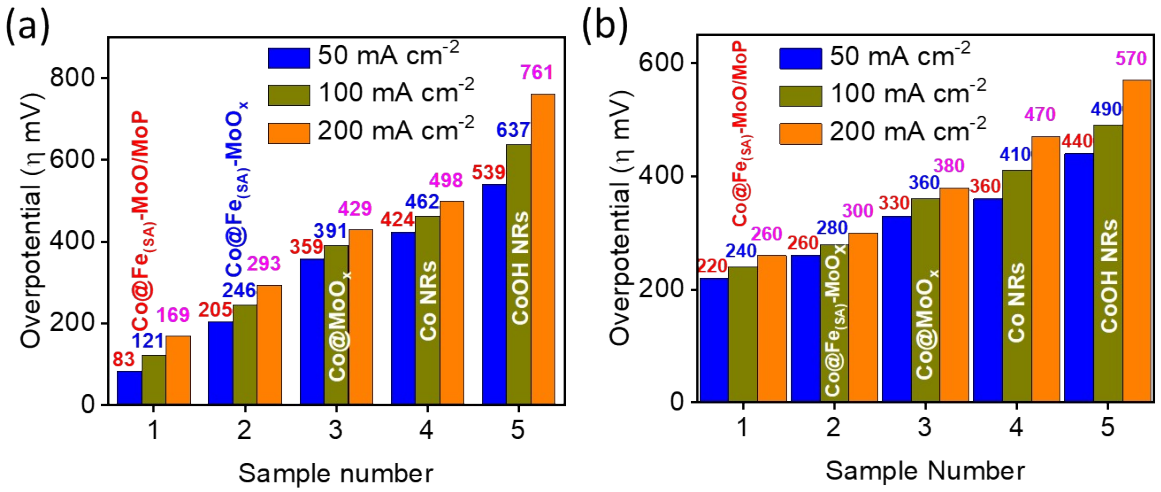

Figure S19. Overpotential comparison of the prepared samples towards (a) HER and (b) OER measured at 50, 100 and 200 mA cm^{-2} current density in a natural seawater environment.

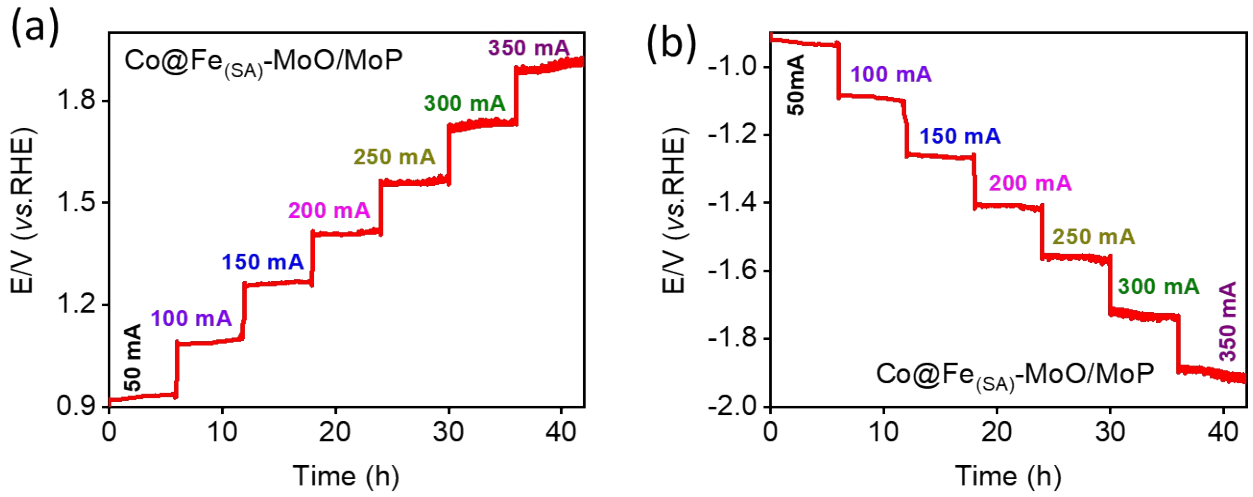

Figure S20. Multi-step of the Co@$Fe_{(SA)}$-MoO/MoP (a)HER and (b) OER in a natural seawater environment.

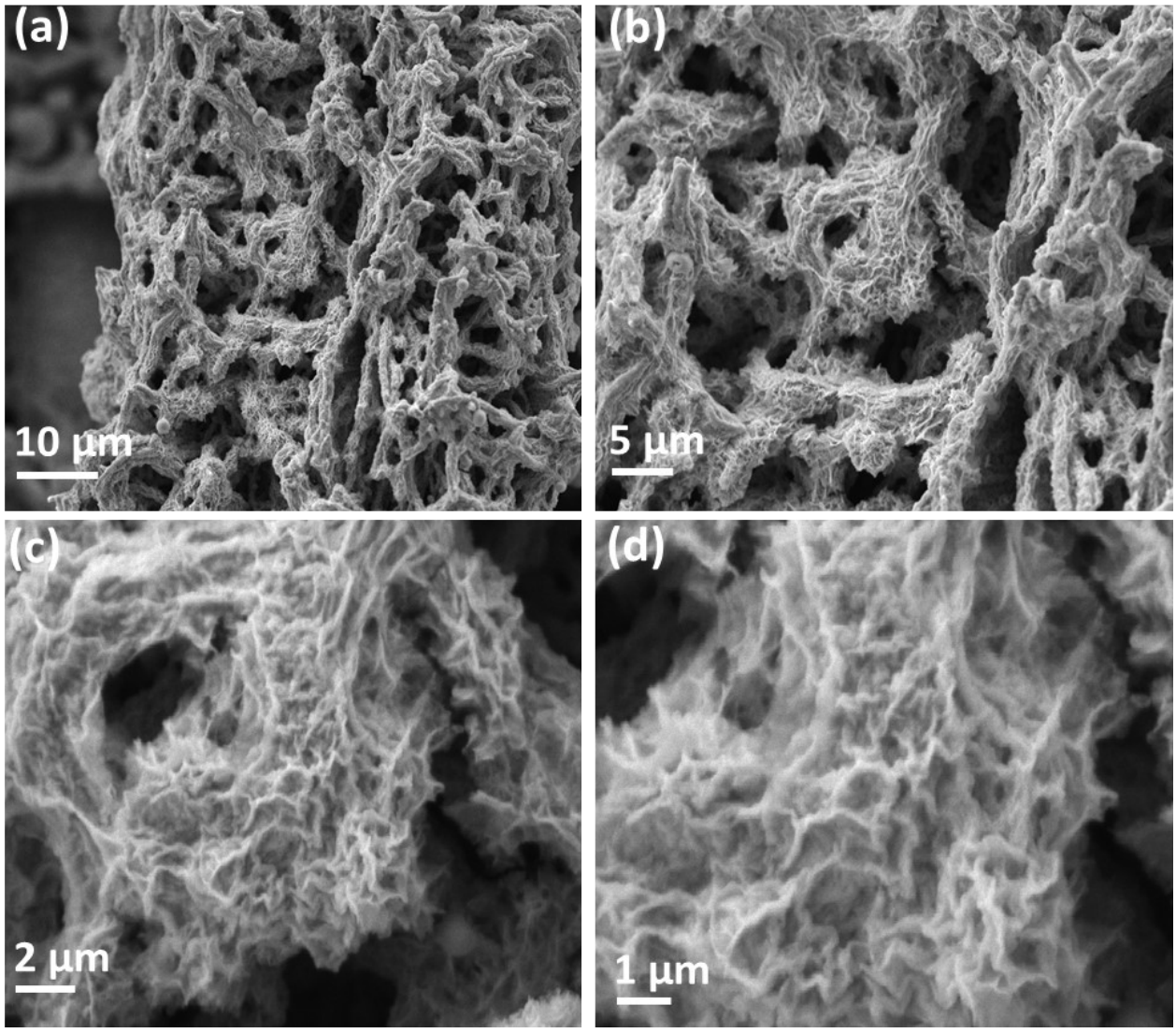

Figure S21. (a-d) FE-SEM images of the Co@$Fe_{(SA)}$-MoO/MoP after HER stability tests at 100 mA cm^{-2} current density

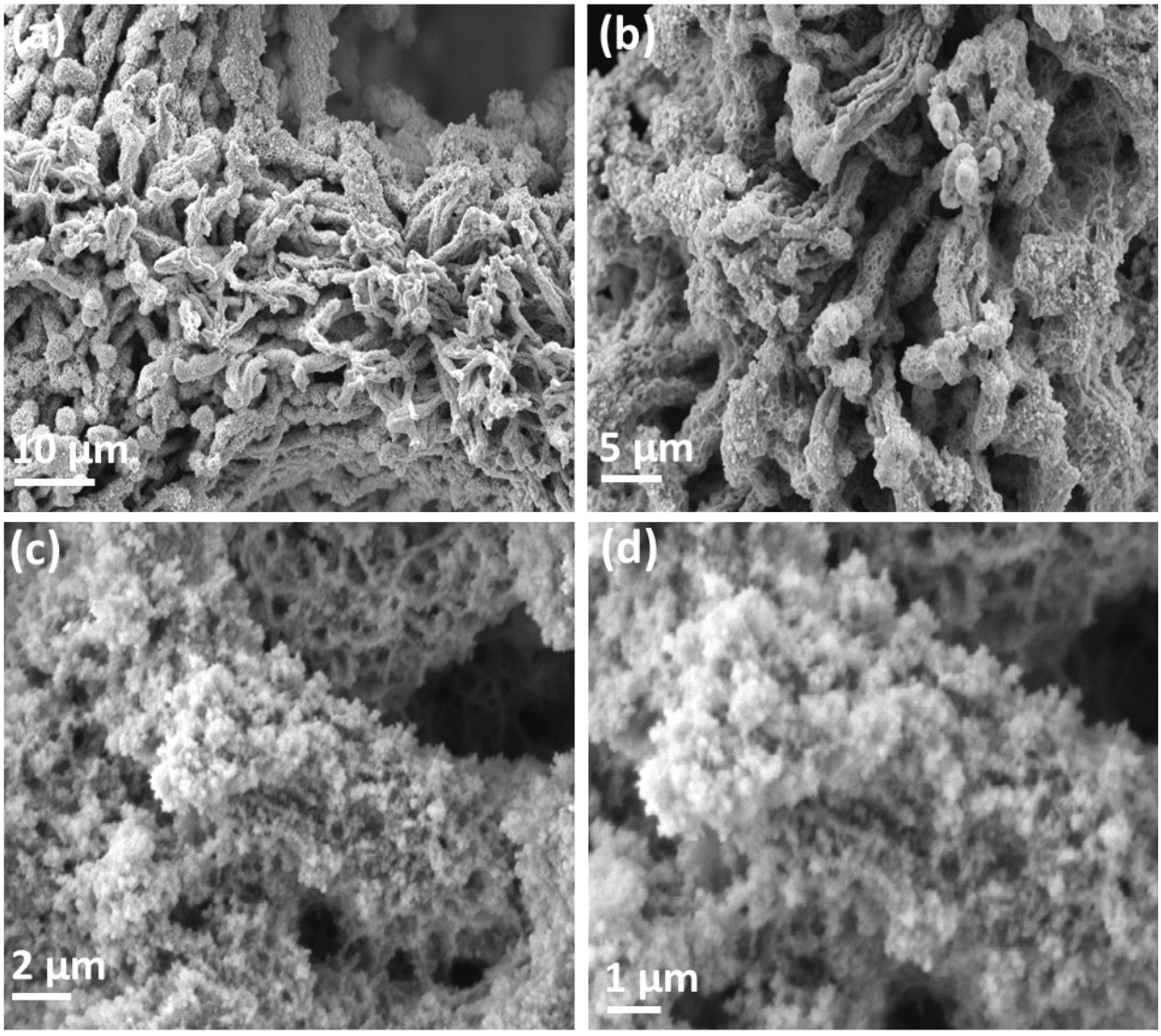

Figure S22. (a-d) FE-SEM images of the Co@$Fe_{(SA)}$-MoO/MoP after OER stability tests at 100 mA cm^{-2} current density

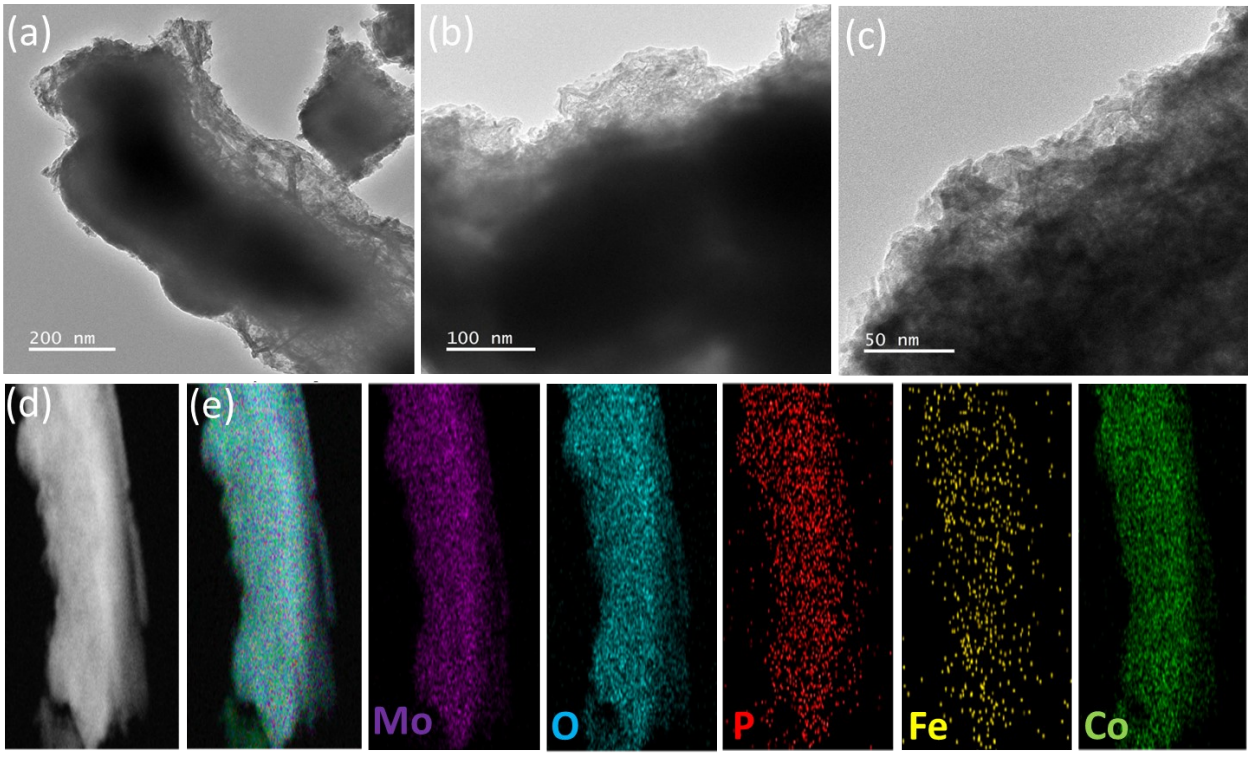

Figure S23. HR-TEM images of the Co@$Fe_{(SA)}$-MoO/MoP after HER stability tests at 100 mA cm^{-2} current density

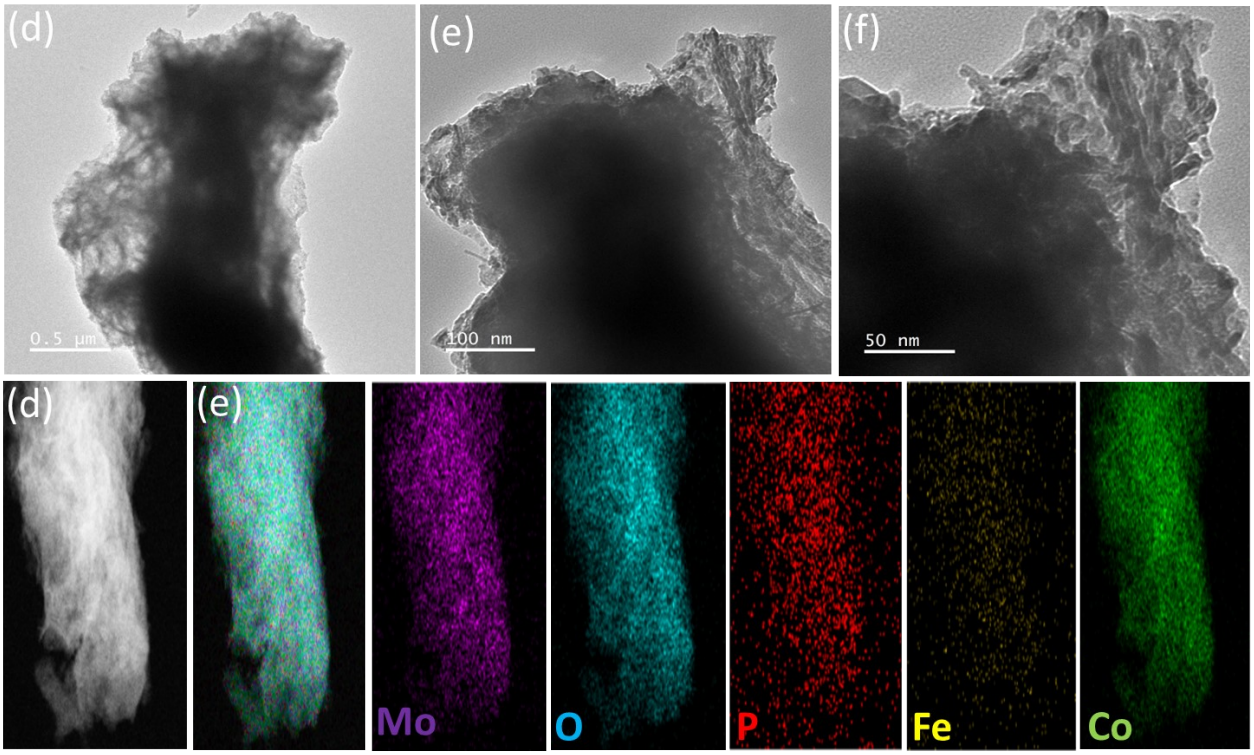

Figure S24.HR-TEM images of the Co@$Fe_{(SA)}$-MoO/MoP after OER stability tests at 100 mA cm^{-2} current density

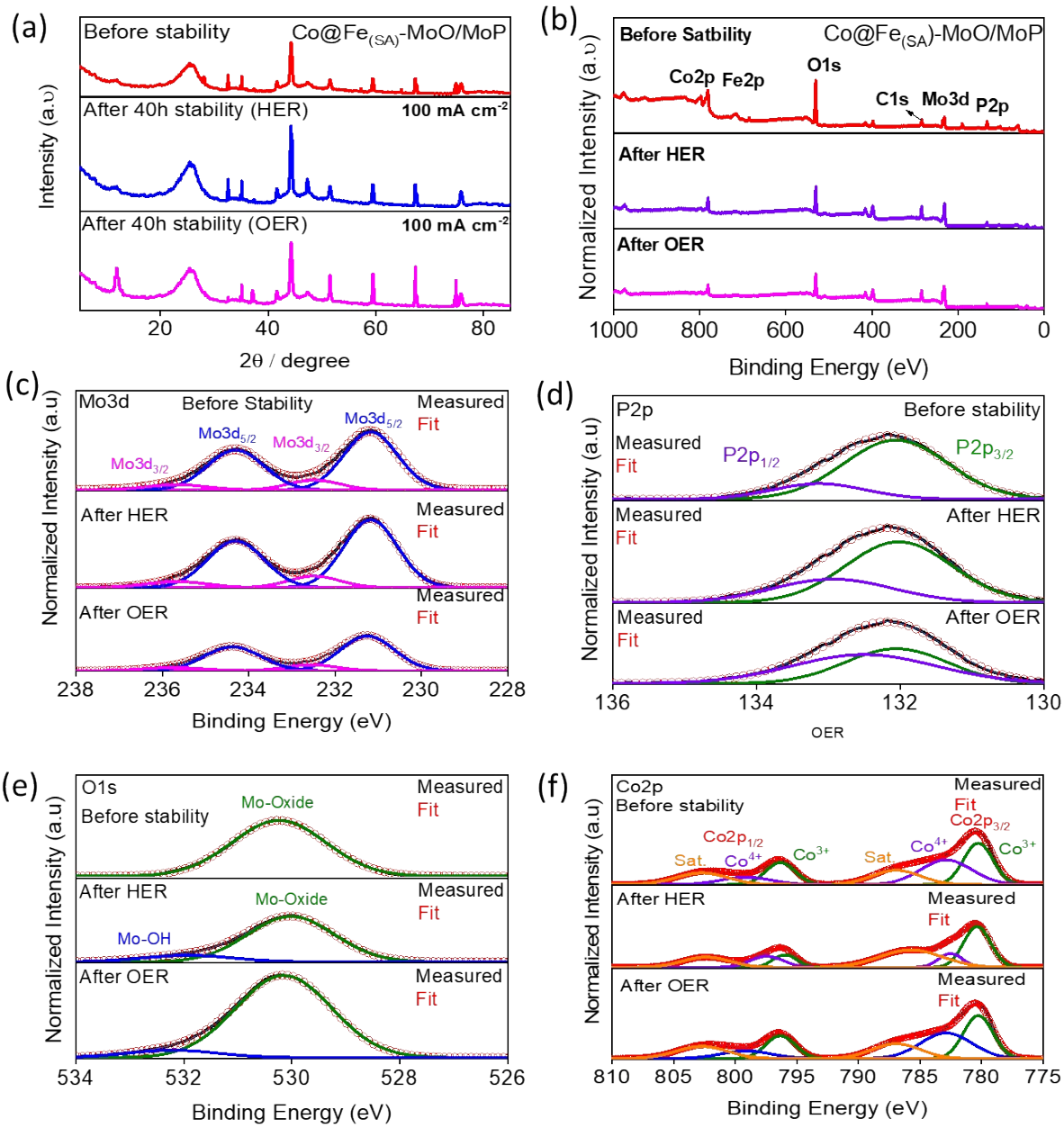
(a)
Before stability
Co@Fe(SA)-MoO/MoP
After 40h stability (HER)
100 mA cm-2
After 40h stability (OER)
100 mA cm-2
Intensity (a.u)
20
40
60
80
2θ / degree
(b)
Before Satbility
Co@Fe(SA)-MoO/MoP
Co2p
Fe2p
O1s
C1s
Mo3d
P2p
After HER
After OER
Normalized Intensity (a.u)
1000
800
600
400
200
0
Binding Energy (eV)
(c)
Mo3d
Before Stability
Mo3d5/2
Mo3d3/2
Measured
Fit
After HER
After OER
Normalized Intensity (a.u)
238
236
234
232
230
228
Binding Energy (eV)
(d)
P2p
Before stability
P2p1/2
P2p3/2
Measured
Fit
After HER
After OER
Normalized Intensity (a.u)
136
134
132
130
OER
(e)
O1s
Before stability
Mo-Oxide
Mo-OH
Measured
Fit
After HER
After OER
Normalized Intensity (a.u)
534
532
530
528
526
Binding Energy (eV)
(f)
Co2p
Before stability
Co2p1/2
Co2p3/2
Sat.
Co4+
Co3+
Measured
Fit
After HER
After OER
Normalized Intensity (a.u)
810
805
800
795
790
785
780
775
Binding Energy (eV)

Figure S25. (a) XRD patterns of Co@$Fe_{(SA)}$-MoO/MoP sample before and after long-term HER/OER stability tests conducted at ~100 mA cm^{-2} current density; (b) XPS survey scan comparison of Co@$Fe_{(SA)}$-MoO/MoP samples before and after HER/OER stability tests and with high-resolution peak deconvolutions of (c) Mo3d, (d) P2p, (e) O1s, and (f) Co2p.

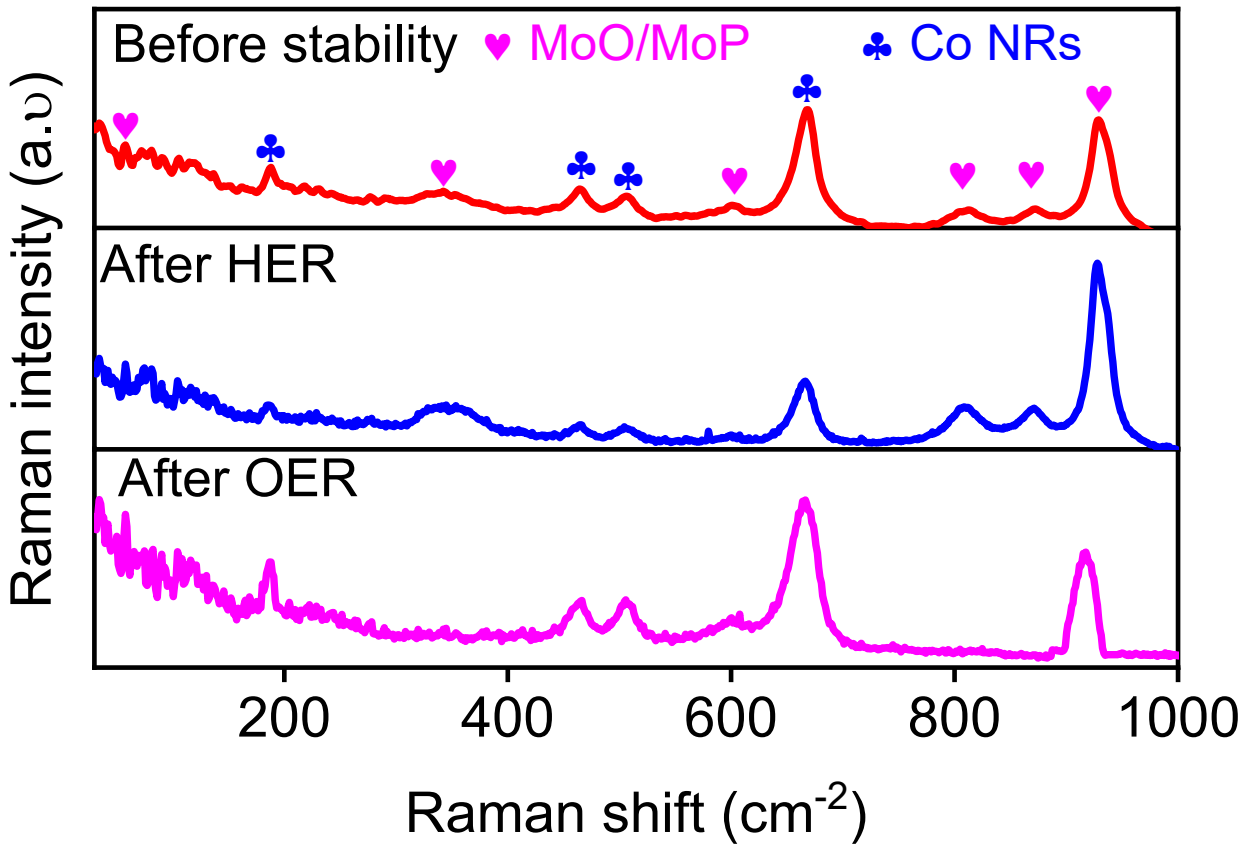

Figure S26.Raman spectra comparison of Co@$Fe_{(SA)}$-MoO/MoP sample before and after HER and OER stability measured at 100 mA cm^{-2} current density in natural seawater.

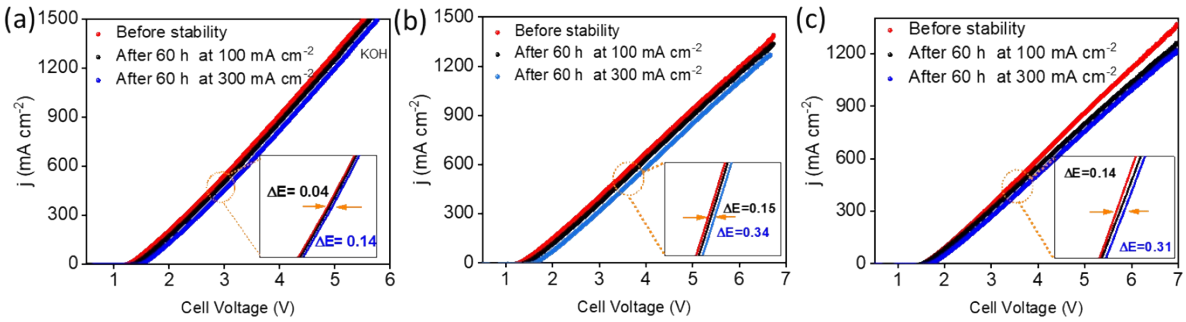

Figure S27. LSV curves of the Co@$Fe_{(SA)}$-MoO/$MoP_{(-/+)}$ measured after long-term stability tests conducted in different electrolytes (a) KOH,(b) Natural seawater and (c) Simulated seawater at 100 mA cm^{-2} and 300 mA cm^{-2} current density, respectively

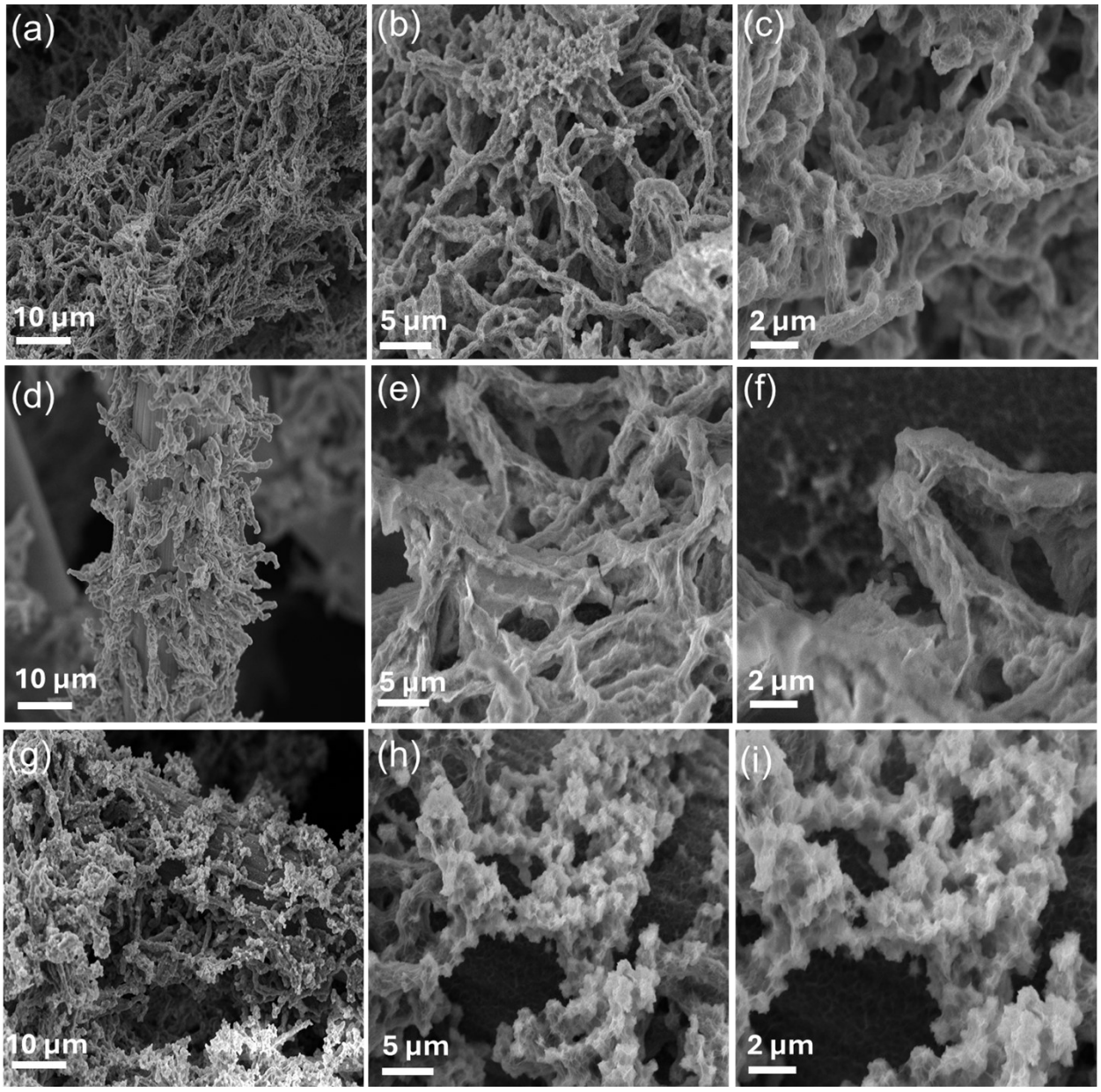

435

436 **Figure S28.** FE-SEM images of Co@$Fe_{(SA)}$-MoO/MoP after device stability tests in different

437 electrolytes: (a-c) 1.0 M KOH, (d-f) simulated seawater, and (g-i) natural seawater, showing the

438 morphological changes after prolonged testing.

439

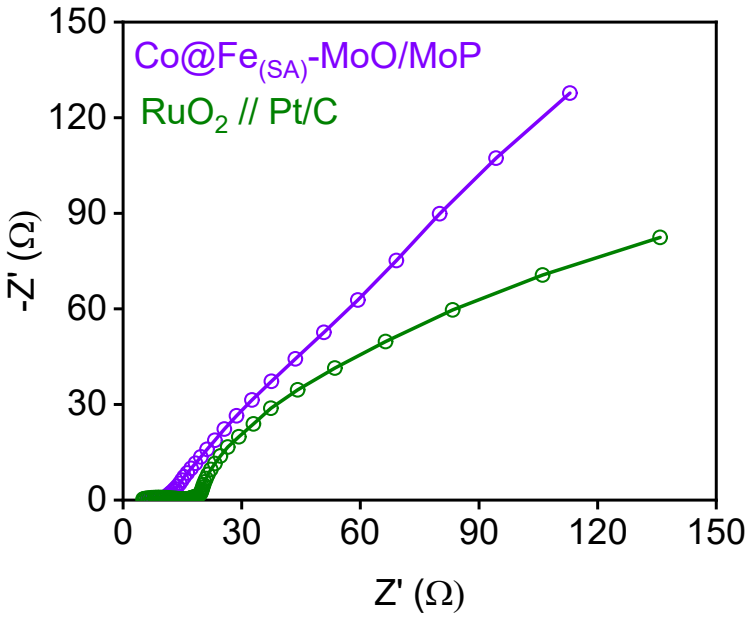

440

441 **Figure S29.** Nyquist plots of impedance spectra at 2.11 V

Table S1.Comparison of the HER overpotentials in 1.0 M KOH between Co@$Fe_{(SA)}$-MoO/MoP and recent reported electrocatalysts.

Catalysts	η_{100} (mV)	η_{200} (mV)	Tafel slope (mV dec^{-1})	References
Co@$Fe_{(SA)}$-MoO/MoP	**36**	**57**	**32**	***This work***
$NiP_2/NiSe_2$	89 η_{10}	160 η_{10}	65.7	*Appl. Catal. B Environ. 282 (2021) 119584*
0.02 Ni-MoP	162η_{10}		102.6	*Nano Energy. 70 (2020) 104445*
$CoO/CoMoO_3/Co_2Mo_3O_8$	51η_{10}	195η_{10}	66	*Nanoscale, 15 (2023) 15219–15229*
Mo–NiCoP-3	148η_{100}	..	60	*Nano-Micro Lett. (2019) 11:55*
$Mo(NiFeCo)_4/Ni$	…	200 η_{2300}	35	*Adv. Funct. Mater.33 (2023) 2214412*
$MoS_2/NiPS_3$	112 η_{10}		64	*Adv. Mater. 34 (2022) 2203615*
10:MoCo-VS_2	63η_{10}		50	*J. Mater. Chem. A, 10 (2022) 9067-9079.*
N-MoS_2·Ni_3S_2/NiS	70η_{10}		95.2	*J. Mater. Chem. A, 10 (2022) 11755-11765.*
Ni_3Mo_3C@NPC NWs/CC	215η_{100}	…	30.9	*ChemSusChem 2018, 11, 2717 – 2723*
FeCoNiMo HEA	250η_{10}		48.02	*ACS Catal. 12 (2022) 10808−10817.*
Mo-NiPx/NiSy	137η_{10}	182η_{10}	49	*Adv. Funct. Mater. 31 (2021) 2101532.*
Mo-/Co-N-C	…	230 η_{1000}	47	*Adv. Funct. Mater. 31 (2021) 2102285.*

Table S2. Comparison of the OER overpotentials in 1.0 M KOH between Co@$Fe_{(SA)}$-MoO/MoP and recent reported electrocatalysts.

Catalysts	**η_{100} (mV)**	**η_{200} (mV)**	**Tafel slope**	**References**
Co@$Fe_{(SA)}$-MoO/MoP	**270**	**290**	**38**	***This work***
NW-$MnCo_2O_4$/GDY/CC	338^{η}_{10}	482^{η}_{10}	111	*Adv. Funct. Mater. 32 (2022) 2107179*
$Co_3O_{3.87}F_{0.13}$	430^{η}_{10}		56	*Appl. Catal. B Environ. 281 (2021) 119535*
NiP_2/$NiSe_2$	250^{η}_{10}	329^{η}_{10}	71.65	*Appl. Catal. B Environ. 282 (2021) 1195842*
Co_3Mo/$CoMoO_x$	256^{η}_{10}	-	65.3	*Chemical Engineering Journal 431 (2022) 133240*
Co_2P/CoNPC	326^{η}_{10}	-	78	*Adv. Mater. 32 (2020) 2003649*
$NiSe_2$/$CoSe_2$-N	286^{η}_{10}	-	53	*Adv. Mater. 32 (2020) 2000607*
E-Mo–NiCoP-3	$364_{\eta 100}$			*Nano-Micro Lett. (2019)*
MoO_3/Ni–NiO	-	347^{η}_{10}	60	*Adv.Mater. 32 (2020) 2003414*
MoS_2/$NiPS_3$	$30_{\eta 20}$		86	*Adv. Funct. Mater. 34 (2023) 2214412.*
$NiCo_2O_4$/$Co_{5.47}N$		$310_{\eta 50}$	55.1	*Small 16 (2020) 1906775.*

449

450 **Table S3**. EIS Nyquist plot fitting parameters of the synthesis catalysts in 1.0 M KOH

Materials	R_s (Ω)	C_1 (F)	R_{ct} (Ω)	Q_1 (Ω ·s^n, n)
Co@$Fe_{(SA)}$-MoO/MoP	1.96	0.0006217	0.68	0.0008523
Co@$Fe_{(SA)}$-MoO_x	2.76	0.0008257	0.95	0.84
Co@MoO_x	1.88	0.000896	1.09	0.0001357
Co NRs	2.53	0.0009587	1.89	0.00088
Co-OH NRs	3.024	0.0009877	2.16	0.0006938,0.58

451

Table S4.Performance comparison of our developed AEMWE with other recently reported AEMWEs.

Cathode catalyst	**Anode catalyst**	**Condition**	**AEMWE Perfomance**	**References**
Co@$Fe_{(SA)}$-MoO/MoP	Co@$Fe_{(SA)}$-MoO/MoP	1M KOH @25 ^{0}C	0.5A cm^{-2} @2.11 V	*This work*
NiFeS@Ti_3C_2	NiFeS@Ti_3C_2	1 M KOH @ 55° C	0.4 A cm^{-2} @ 1.85 V	*Appl. Catal. B 2023, 321, 122039.*
Pt/C	NiCoFe-NDA	1 M KOH @ 50° C	0.325 A cm^{-2} @ 1.8 V	*Energy Environ. Sci.* ***2021****, 14, 6546.*
Ru_2P NFs	IrO_2	1 M KOH @ 50° C	1 A cm^{-2} @ 1.86 V	*Chem. Eng. J.* **2021**, *420*, 130491.
$MoO_2/MoNi_4$	HS-RuCo/NC	1 M KOH	1 A cm^{-2} @ 2.07 V	*Small* ***2023****, 19, 2207611.*
NiFeCr-LDH	Ag NP	1 M KOH @ 40° C	0.2 A cm^{-2} @ 2.21 V	*Small* **2022**, *18*, 2200303.
MoO_2/Ni	Ni foam	1 M KOH @ 60° C	0.55 A cm^{-2} @ 2 V	*J. Mater Chem. A* **2023**, *11*, 5789.
NiFeCo/ Nickel Fiber Paper	$NiFe_2O_4$/ Stainless-	1 M KOH @ 50° C	0.88 A cm^{-2} @ 2.2 V	*J. Mater. Chem. A 2022, 10, 8401.*

	Steel			
B,V-Ni_2P	NiFeOOH	1 M KOH @ 50° C	1 A cm^{-2} @ 1.92	*Small* **2023**, *19*, 2208076.
Ni-Co-S/CP	IrO_2	1 M KOH @ 50° C	1.7 A cm^{-2} @ 2.4 V	*Int. J. Energy Res.* **2021**, *45*, 1918.

455

Reference

1 X. Zhu, K. Dong, D. C. Nguyen, S. Prabhakaran, D. H. Kim, D. T. Tran, N. H. Kim and J. H. Lee, *J Mater Chem A Mater*, DOI:10.1039/d4ta02881c.

2 P. P. Dhakal, U. N. Pan, M. R. Kandel, R. B. Ghising, S. Prabhakaran, D. H. Kim, N. H. Kim and J. H. Lee, *Compos B Eng*, DOI:10.1016/j.compositesb.2024.111640.

3 N. K. Shrestha, S. A. Patil, J. Han, S. Cho, A. I. Inamdar, H. Kim and H. Im, *J Mater Chem A Mater*, 2022, **10**, 8989–9000.

4 M. R. Kandel, U. N. Pan, P. P. Dhakal, R. B. Ghising, T. T. Nguyen, J. Zhao, N. H. Kim and J. H. Lee, *Appl Catal B*, DOI:10.1016/j.apcatb.2023.122680.

5 P. K. L. Tran, T. H. Nguyen, D. T. Tran, V. A. Dinh, T. T. Nga Ta, C. L. Dong, N. H. Kim and J. H. Lee, *Appl Catal B*, DOI:10.1016/j.apcatb.2024.124801.

6 K. D. Tran, T. H. Nguyen, D. T. Tran, V. A. Dinh, N. H. Kim and J. H. Lee, *ACS Nano*, 2024, **18**, 16222–16235.

7 P. E. Blochl, *Projector augmented-+rave method*, vol. 50.

8 J. P. Perdew, K. Burke and M. Ernzerhof, *Generalized Gradient Approximation Made Simple*, 1996.

9 G. Kresse and J. Furthmü, *Efficient iterative schemes for ab initio total-energy calculations using a plane-wave basis set*, 1996.

10 S. Grimme, J. Antony, S. Ehrlich and H. Krieg, *Journal of Chemical Physics*, DOI:10.1063/1.3382344.